Spectroscopic Characterization of Nonnative Conformational States of Cytochrome *c*

Silke Oellerich,[‡,#] Hainer Wackerbarth,[‡,¶] and Peter Hildebrandt*[,‡,§]

Max-Planck-Institut für Strahlenchemie, Stiftstrasse 34-36, D-45470 Mülheim, Germany, and Instituto de Tecnologia Química e Biológica, Apartado 127, Av. da República, 2781-901 Oeiras, Portugal

Received: October 17, 2001; In Final Form: March 28, 2002

Protein and heme structural changes of ferric and ferrous cytochrome *c* (Cyt-*c*) that are induced by electrostatic binding (e.g., liposomes, electrodes), by hydrophobic interactions (e.g., monomeric sodium dodecyl sulfate), by guanidium hydrochloride (GuHCl), and at low pH and high temperature were studied by UV−vis absorption, circular dichroism (CD), electron paramagnetic resonance (EPR), and (surface-enhanced) resonance Raman [(SE)RR] spectroscopy. In a global spectral analysis, all species that differ with respect to the heme structure were identified and characterized in terms of the spin and ligation state of the heme as well as of protein secondary and tertiary structure changes. The results indicate that the upper part of the heme pocket including the Met-80 ligand is the most labile protein region such that this ligand is dissociated from the heme iron in all nonnative Cyt-*c* states. Among these states, there are two six-coordinated low-spin (LS) configurations with H_2O or His-33 serving as the sixth (axial) ligand. Whereas the ferric H_2O/His-18-ligated low-spin species is only formed in the A state at low pH and high ionic strength, the His-33/His-18-ligation pattern corresponds to a stable ferric configuration inasmuch as it can be induced by electrostatic and hydrophobic interactions and under nondenaturing and denaturing conditions, that is, nearly independent of the secondary structure. Conversely, the heme pocket on the opposite side of the heme remains largely preserved except for ferric Cyt-*c* at very low pH and high GuHCl concentrations as indicated by the replacement of His-18 by a water molecule. Structural changes that are localized in the heme pocket and lead to a ferric bis-His-coordinated LS, a ferric water/His and mono-His high-spin (HS), and a ferrous mono-His HS configuration may be induced by hydrophobic or electrostatic interactions with the front surface of Cyt-*c*. The present study contributes to a consistent description of the conformational manifold of Cyt-*c*, which is essential for elucidating the role of conformational transitions during the natural functions of Cyt-*c* in energy transduction and apoptosis.

I. Introduction

Conformational transitions of proteins are known to play a crucial role in many biochemical and biophysical reactions that are associated with catalytic and transport processes, regulation of biological activity, and signal and energy transduction.[1] Clearly, a deeper understanding of the molecular mechanisms of these processes requires a detailed analysis of the conformational equilibria and dynamics of the proteins as well as of the structures of the various conformational states. This challenging task is linked to the more general problem of elucidating mechanisms and patterns of protein folding.[2] In this respect, cytochrome *c* (Cyt-*c*) has increasingly attracted the interest of researchers in this field. On one hand, this small soluble monoheme protein has been found to be a convenient model protein for polypeptide folding studies that are dedicated to the understanding of general principles of these fundamental processes (e.g., refs 3−6). On the other hand, Cyt-*c* exerts quite different biological functions that appear to be associated with specific conformational transitions.

Cyt-*c*'s function as an electron carrier in the respiratory chain of an aerobic organism has been known for a long time.[7,8] It transfers electrons to the membrane-bound enzyme complex cytochrome *c* oxidase (CcO), which reduces oxygen to water. Considerable efforts have been made to elucidate the mechanism of the interprotein electron-transfer process. Circular dichroism (CD), magnetic CD, and resonance Raman (RR) spectroscopic studies on the interactions of Cyt-*c* and CcO have shown that in the electrostatically stabilized fully oxidized and fully reduced Cyt-*c*/CcO complexes structural changes of the individual redox sites are induced.[9−12] By comparison of the RR spectra, the alterations of the heme pocket structure of Cyt-*c* were attributed to a conformational state that is also formed when Cyt-*c* binds to anionic surfaces of phospholipid vesicles, micelles, polyanions, and electrodes.[13−16] In this conformational state, denoted as B2, the axial Met-80 ligand is replaced by another strong-field ligand that was previously assigned to a hydroxide.[11,17] Because state B2 exhibits a much more negative redox potential than the native state B1,[15,18] it was suggested that the redox process of Cyt-*c* and CcO is controlled by conformational transitions.[11]

More recently, a second biological function of Cyt-*c* has been discovered. It was shown that during apoptosis Cyt-*c* is transferred from the intermembrane space to the cytosol where it constitutes an activator for caspase-9, one of the essential enzymes in the reaction cascades of programmed cell death.[19−21] Jemmerson et al.[22] have demonstrated that apoptotic Cyt-*c* is complexed by monoclonal antibodies that bind to the region

* To whom correspondence should be addressed. Instituto de Tecnologia Química e Biológica, Apartado 127, Av. da República, 2781-901 Oeiras, Portugal. Tel: +351 21 446 9741. Fax: +351 21 441 1277. E-mail: hildebrandt@itqb.unl.pt.

‡ Max-Planck-Institut für Strahlenchemie.

Present address: Leiden University, Huygens Laboratory, Department of Biophysics, Niels Bohrweg 2, 2333 CA Leiden, The Netherlands.

¶ Present address: Danmarks Tekniske Universitet, Biouorganisk Kemi, Bygning 207, 2800 Lyngby, Denmark.

§ Instituto de Tecnologia Química e Biológica.

10.1021/jp013841g CCC: $22.00
Published on Web 06/05/2002

around Pro-44. These antibodies also recognize Cyt-*c* immobilized to phospholipid vesicles but do not form complexes with Cyt-*c* in solution. Thus, it is likely that, specifically in the region of Pro-44, both apoptotic and lipid-bound Cyt-*c* exhibit a similar conformation, which differs from that of native Cyt-*c*.

Consequently, the common aspect of the two quite different biological functions of Cyt-*c* is that they are obviously associated with transitions to conformational states, which are structurally different from the native Cyt-*c* and are, therefore, denoted as nonnative states. Obviously, these nonnative conformational states of Cyt-*c* can also be obtained in model systems that mimic the intermolecular interactions of the biological environment. Such model systems are spectroscopically "silent" for many techniques and, thus, allow studying the conformational transitions of Cyt-*c* in a detailed and systematic manner.

However, despite the large number of experimental studies in this field, there is no uniform and consistent picture about (i) the kind of intermolecular interactions and the parameters that induce specific conformational states of Cyt-*c*, (ii) the structural changes in these nonnative states, and (iii) the thermodynamics and dynamics of the various conformational transitions. The present study is a contribution to fill this gap. First, we have employed different spectroscopic methods including far- and near-UV−CD, RR, surface-enhanced RR (SERR), electron paramagnetic resonance (EPR), and UV−vis absorption spectroscopy. These techniques provide complementary information of the protein conformation on the secondary and tertiary structure level as well as of the heme (pocket) structure. Second, we have chosen model systems that exert qualitatively different interactions with Cyt-*c*. Sodium dodecyl sulfate (SDS) micelles and electrodes covered with specifically adsorbed anions provide anionic surfaces for electrostatic interactions with the lysine-rich domain around the heme crevice of Cyt-*c*.[13,18] Conversely, hydrophobic interactions prevail in the case of monomeric SDS.[23] Cyt-*c* binding to phospholipid vesicles is predominantly electrostatic in nature but may also involve hydrophobic forces at high surface coverage.[24−26] Third, we have extended the studies to conformational transitions induced by guanidinium hydrochloride (GuHCl), low pH, and elevated temperature to identify similarities and differences with those conformational changes that occur under much milder conditions. Furthermore, particularly for the GuHCl- and acid-induced conformational transitions, our own results can be compared with a large set of previously published data (e.g., refs 4, 6, 27, and 28 and references therein), which may serve as a reference for the overall analysis of the conformational flexibility of Cyt-*c*. Fourth, the present study was carried out for both ferric and ferrous Cyt-*c* to characterize the redox-linked differences in the conformational stability of this protein.

II. Materials and Methods

Materials. Horse heart cytochrome *c* was purchased from Sigma and used without further purification if not stated otherwise. The protein was dissolved in 5 mM HEPES and 1 mM EDTA buffer (pH 7) for experiments with dioleoylphosphatidylglycerol (DOPG) liposomes and in 50 mM phosphate buffer (pH 7) for all other experiments. Yeast iso-1 cytochrome *c* was expressed and purified as described elsewhere.[11] All other chemicals used were of the highest-purity grade available.

Vesicle Preparation. DOPG was purchased from Sigma. Dry films of 10 mg lipid were prepared from a stock solution in chloroform under a nitrogen stream and left under vacuum for at least 8 h to remove all traces of the organic solvent. The lipid films were resuspended in HEPES/EDTA and gently vortexed for a few minutes. DOPG vesicles were then prepared by sequential extrusion through polycarbonate membranes (Osmonics) of decreasing pore size diameter. Vesicle size, homogeneous distribution of vesicle sizes, and vesicle stability were checked by dynamic light scattering (submicron particle analyzer model N4MD, Coulter Electronics).

UV−Vis Absorption Spectroscopy. UV−vis absorption spectra were recorded on a Unicam UV2 spectrophotometer with a spectral resolution of 0.5 nm, a bandwidth of 4 nm, and a scan speed of 600 nm/min. The path length of the optical cell was 10 mm for all experiments.

Resonance Raman and Surface-Enhanced Resonance Raman Spectroscopy. RR and SERR spectra were measured at ambient temperature with the 413-nm excitation line of a Kr^+ laser (Coherent Innova 302) using a spectrograph (U1000, ISA) equipped with a liquid nitrogen cooled CCD camera. The spectral resolution was 4 cm^{-1}, and the step width (increment per data point) was 0.53 cm^{-1}. The power of the incident laser beam focused on the sample was 40 mW. For temperature-dependent RR experiments, the rotating cell was placed in a homemade thermostated chamber allowing temperature control up to 70 °C with an accuracy of ±1 °C. The protein concentration for the RR experiments was 10 μM.

SERR experiments were carried out with a home-built rotating Ag electrode using a three-electrode cell controlled by a potentiostat. The protein concentration in the electrochemical cell was 10^{-7} M in a buffered solution containing 50 mM phosphate buffer (pH 7) and 50 mM Na_2SO_4 as supporting electrolyte. All potentials cited in this paper refer to the saturated calomel electrode. The preparation of the SERR-active surface followed a protocol described previously.[15] After the adsorption of Cyt-*c* at −370 mV, a spectrum was measured to check the integrity of the adsorbed protein. This spectrum was used as a standard for the spectral calibration. The SERR measurements were obtained with iso-1 cytochrome *c*. This protein undergoes essentially the same conformational transitions as horse heart Cyt-*c* and the corresponding SERR/RR spectra reveal only subtle differences in frequencies and relative band intensities.[29] The differences were adequately considered in the global analysis of the RR and SERR spectra (vide infra).

All RR and SERR measurements were repeated several times under the same conditions to ensure reproducibility. To improve the signal-to-noise ratio, the individual spectra were added up only if no spectral differences were noted. Prior to the spectra analysis, contributions from components other than Cyt-*c* (e.g., GuHCl) were subtracted and the structureless background was removed by polynominal subtraction. The spectra that were obtained in this way were analyzed by a band fitting or component analysis.[30]

Circular Dichroism Spectroscopy. Spectra were recorded at ambient temperature on a JASCO J-715 spectropolarimeter. Far-UV CD spectra (190−260 nm) were measured using a quartz cell of 1 mm path length. Near-UV and Soret CD spectra (250−500 nm) were obtained in a quartz cell of 10 mm path length. Four scans were averaged per spectrum. The spectral resolution was 0.5 nm. Furthermore, a bandwidth of 1 nm and a response time of 1 s were typically used.

Electron Paramagnetic Resonance Spectroscopy. X-band EPR spectra (9.6 GHz) were measured with an ESP 300E spectrometer (Bruker) equipped with an ER 041 XK-D microwave bridge (Bruker) and a helium flow cryostat (ESR 910; Oxford Instruments) to maintain a temperature of 10 K. The modulation frequency was set to 100 kHz.

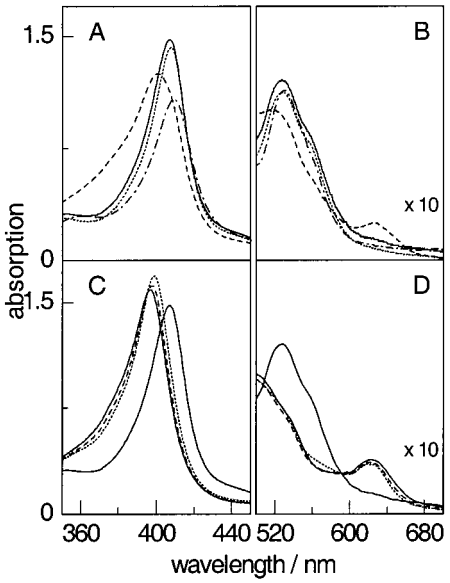

Figure 1. UV−vis absorption spectra of ferric Cyt-*c*. The top panels show Cyt-*c* in aqueous solution at pH 7.0 (− · −), in 2 mM SDS (···), in 500 mM SDS (− − −), and in 6 M GuHCl at pH 7.5 (—). The Soret-band and visible regions are shown in panels A and B, respectively. The bottom panels show Cyt-*c* in GuHCl (6 M) solution at pH 7.5 (—), pH 4.1 (···), pH 3.3 (− − −), and pH 0.9 (− · −). The Soret-band and visible regions are displayed in panels C and D, respectively.

III. Results and Discussion

UV−Vis Absorption and Resonance Raman Spectral Changes of Ferric Cytochrome *c* Induced by SDS and GuHCl. The UV−vis absorption spectrum of native ferric Cyt-*c* displays the characteristic Soret band at 409 nm and a weaker broad Q band at ca. 528 nm, both originating from the porphyrin chromophore (Figure 1). In addition, a very weak band at 695 nm is observed, which is assigned to a S(Met) → Fe charge-transfer transition and, hence, is indicative for the native His/Met ligation pattern of the heme.[31]

Addition of SDS to ferric Cyt-*c* causes a blue-shift of the Soret-band absorption maximum, which is relatively small (2 nm) up to an SDS concentration of 2 mM, that is, the critical micelle concentration (cmc) in 50 mM phosphate solution at pH 7. Between 2 and 5 mM, the shift becomes substantially larger and the Soret-band maximum is found at 402 nm, which remains nearly unchanged even upon further increasing the SDS concentration to 500 mM (Figure 1). Concomitant to the shift of the Soret-band maximum, the intensity of the 695-nm band decreases (cf. ref 32). For SDS concentrations ≥2 mM, this band disappears and a new band at ca. 625 nm grows in that is indicative of a high-spin (HS) species. In the Q-band region, we observed a blue shift of the 530-nm band associated with an intensity increase at ca. 490 nm.

The changes in the UV−vis absorption spectrum induced by 6 M GuHCl at pH 7.0 are similar to those observed at a SDS concentration of 2 mM (cf. ref 33). In addition, we note a shoulder of the Q band at ca. 560 nm (Figure 1B). Upon lowering the pH (≤2.2), the Soret-band maximum shifts down to 397 nm (Figure 1C), accompanied by the growing-in of absorption bands at ca. 500 and 622 nm (Figure 1D) that indicate the transformation into HS species.

In aqueous solution at pH 7.0, the heme iron of native Cyt-*c* is axially coordinated by His-18 and Met-80, leading to a six-coordinated low-spin (6cLS) configuration in both the oxidized and the reduced state. This configuration is reflected by the characteristic frequencies of the RR marker bands ν_4, ν_3, ν_2, and ν_{10}, which for the ferric form are at 1372, 1502, 1584, and, 1635 cm^{-1}, respectively (Figure 2A). Addition of GuHCl or 2 mM SDS at pH 7.0 leads to distinct shifts of the RR marker bands to higher frequencies (Figure 2B,C).[4,33] Furthermore, the ν_{11} mode of native ferric Cyt-*c* at 1560 cm^{-1} disappears, and the ν_{10} mode suffers a substantial intensity decrease. Nevertheless, the RR bands remain in the range for a 6cLS configuration,[34,35] and no new bands indicative for a different spin state can be detected. Note that in both GuHCl (6 M) and SDS (2 mM) the RR spectra of Cyt-*c* are essentially identical.

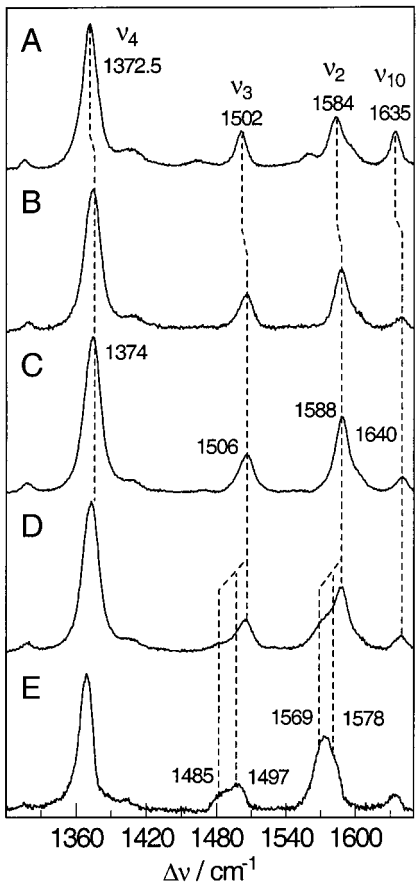

Figure 2. RR spectra of ferric Cyt-*c* in the marker band region between 1300 and 1650 cm^{-1} obtained from different solutions: (A) aqueous, pH 7.0; (B) 6 M GuHCl, pH 7.5; (C) 2 mM SDS, pH 7.0; and (D) 10 mM SDS, pH 7.0. Spectrum E shows a difference spectrum of spectrum D minus spectrum C. The spectra were obtained with 413-nm excitation.

Upon increasing the SDS concentration above 2 mM, a broadening of the band at ca. 1506 cm^{-1} (ν_3) and a distinct shoulder at the low-frequency side of the 1588-cm^{-1} peak (ν_2) are observed (Figure 2D), indicating the formation of one or more additional nonnative species besides the nonnative 6cLS form. Subtracting the RR spectrum measured in the presence of 2 mM SDS (corresponding to the "pure" nonnative 6cLS species) from RR spectra obtained at higher SDS concentrations yields difference spectra such as that shown in Figure 2E. As indicated by the broad and downshifted peaks in the ν_3 and ν_2 mode region, the difference spectrum includes contributions from (at least) two species. Especially, the positions of the maxima of the peak in the ν_3 mode region at 1485 and 1497 cm^{-1} point to a six-coordinated high-spin (6cHS) and a five-coordinated high-spin (5cHS) species. This observation is in line with the characteristic HS band at 625 nm in the UV−vis absorption spectra obtained under the same conditions (vide supra).

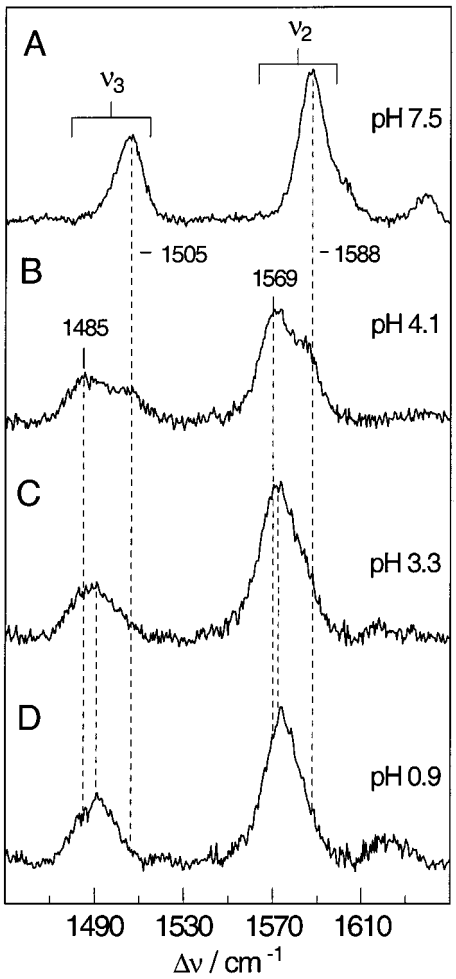

Figure 3. RR spectra of ferric Cyt-*c* in the marker band region between 1450 and 1650 cm^{-1}, obtained from GuHCl (6 M) solutions at different pH: (A) pH 7.5; (B) pH 4.1; (C) pH 3.3; (D) pH 0.9. The spectra were measured with 413-nm excitation.

The formation of HS species in acidic GuHCl solutions is also reflected by the RR spectra (Figure 3) because lowering the pH causes a growing-in of characteristic HS marker bands (e.g., ν_3 at ca. 1485 cm^{-1}) at the expense of the corresponding LS bands (e.g., 1505 cm^{-1}). At pH 4.1, the spectral contributions of the nonnative 6cLS form is still detectable but HS configurations now prevail. At pH 3.3, the 6cLS content is largely reduced and the "HS" peak has changed the shape and the maximum. Upon further lowering of the pH, the 6cLS species vanishes completely and the "HS" peak maximum shifts up to ca. 1493 cm^{-1} (Figure 3D). A comparable pH-dependent variability of the HS signals is noted in the ν_2 and ν_{10} mode regions indicating different HS species. More information about the number and the ligation state of these species is obtained by mutual subtraction of the various spectra measured in the pH range between 4.1 and 0.9. These difference spectra demonstrate the coexistence of one 5cHS and two 6cHS forms in this pH range.

For the qualitative and quantitative (vide infra) analysis of the conformational changes in SDS and GuHCl solutions, the component analysis to the RR spectra has been shown to be the most reliable approach. In this method, the measured spectra are simulated by complete component spectra, each of them representing a distinct species that differs by its RR band pattern. In the first step, the minimum number of contributing species and their approximate component spectra have to be determined. Subsequently, these initial spectra are iteratively refined in a global fit to all measured spectra.[30]

As shown above, GuHCl induces the formation of (at least) four RR-distinguishable heme configurations which in view of the unfolded protein structure (vide infra) are denoted as U species, U[6cHS(1)], U[6cHS(2)], U[5cHS], and U[6cLS] (Table 1). The component spectrum of U[6cLS] can be well approximated by the RR spectrum measured from the Cyt-*c*/GuHCl sample at pH 7.5 (Figure 2B). Initial component spectra for the HS species, U[5cHS], U[6cHS(1)], and U[6cHS(2)], were obtained by mutual subtraction of the measured spectra obtained at different pH. The component spectra of the U species as well as that of the native state, denoted as B1 (B1[6cLS]; Figure 2A) constitute the start set for simulating all RR spectra measured from samples in the presence of GuHCl and different pH. After iterative refinement of the spectral parameters for the U species, a good and consistent global fit was obtained. The fit was substantially worse when only one 6cHS configuration was considered because no component spectrum could be refined that was adequate to reproduce the characteristic 6cHS signals in the entire pH range. These findings a posteriori confirm the conclusion that in acid GuHCl solution two different 6cHS species are formed.

The inspection of the experimental spectra of Cyt-*c* measured in the presence of SDS has revealed a 6cLS, a 5cHS, and a 6cHS configuration in analogy to the Cyt-*c*/GuHCl system. Unlike GuHCL, SDS does not cause a complete unfolding of the protein (vide infra) so that the states observed in SDS solutions are denoted as "B2" states, in analogy to the spectral changes observed for Cyt-*c* bound to phospholipid vesicles or electrodes.[11,15] However, regardless of the obvious differences in the protein structure, we have taken the component spectra of the four U species and that of B1[6cLS] as initial component spectra for the global analysis of the RR spectra measured from Cyt-*c* samples with different SDS concentrations. Whereas the characteristic 6cLS signals could well be reproduced by a superposition of the component spectra of the B1[6cLS] and U[6cLS], substantial discrepancies were noted for the 5cHS marker bands so that the spectral parameters for this species had to be modified to achieve a good global fit. These results imply that the RR spectra of the nonnative 6cLS species induced by SDS and GuHCl, that is, B2[6cLS] and U[6cLS], are nearly identical whereas the component spectrum of U[5cHS] clearly differs from that of the 5cHS form in Cyt-*c*/SDS, which is denoted as B2[5cHS]. No refinements were necessary for the U[6cHS(1)] and U[6cHS(2)] component spectra. Furthermore, using only one of these 6cHS component spectra resulted in a much poorer global fit that could only be improved again by modifying the spectral parameters of the 6cHS component under consideration. Thus, equally good fits could be achieved either by taking into account the same 6cHS species as in Cyt-*c*/GuHCl or by including a single 6cHS species that differs from both U[6cHS(1)] and U[6cHS(2)]. Because of the relatively small spectral contribution(s) of the 6cHS component(s) in these samples, the spectral analysis does not allow an unambiguous distinction between these alternatives. For the sake of simplicity, we adopt the approach involving U[6cHS(1)] and U[6cHS(2)] rather than to postulate a new 6cHS species (Table 1). The component spectra of the ferric U- and B2-state heme configurations are shown in Figure 4.

UV−Vis Absorption and Resonance Raman Spectral Changes of Ferric Cytochrome *c* Induced by Binding to Phospholipid Vesicles. Binding to DOPG liposomes at a lipid/protein ratio of 50:1 (lipid concentration of 500 μM) induces a shift of the Soret-band absorption maximum from 409 to 407.5 nm (Figure 5A). Upon increasing the DOPG concentration, a

TABLE 1: Heme Configurations of Nonnative States of Cyt-*c* in Different Systems

Ferric Heme Configurations

system[a]	B2[5cHS]	B2[6cHS] U[6cHS(1)]	B2[6cLS] U[6cLS]	U[6cHS(2)]	U[5cHS]	A[6cLS]	T[6cLS]
Ag electrode	X	X	X	(?)[b]	(?)[b]		
DOPG vesicles	X	X	X				
SDS	X	X	X	X			
GuHCl	(X)[c,d]	X[d]	X	X[d]	X[d]		
acid, low *I*	(X)[c]	X	X	X	X	(X)[c]	
acid, high *I*	X	X	(X)[c]			X	
high *T*							X

Ferrous Heme Configurations

system	B2[5cHS(1)]	B2[5cHS(2)]	B2[6cLS]	U[6cLS]
Ag electrode	X	(?)[b]	X	
DOPG vesicles	X	X	(X)[c]	
SDS	X	(X)[c]	(X)[c]	
GuHCl	X[d]	X[d]		X

[a] Abbreviations: *I*, ionic strength; *T*, temperature. [b] Minor contributions from these species cannot be ruled out. [c] The contributions of these species did not exceed 10%. [d] In acidic GuHCl solutions.

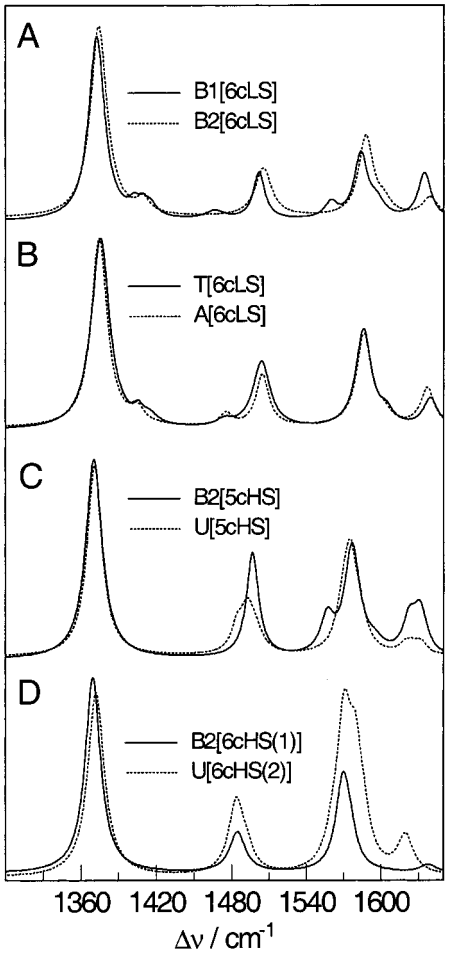

Figure 4. Component RR spectra of the ferric Cyt-*c* species in the marker band region between 1300 and 1650 cm^{-1}. (A) B1[6cLS] (—) and B2[6cLS(1)] (···); (B) A[6cLS] obtained in acid solutions at high ionic strength (···) and T[6cLS] obtained at high temperatures (—); (C) B2[5cHS] (—) and U[5cHS] (···); (D) B2[6cHS(1)] (—) and U[6cHS(2)] (···). Further details are given in the text (cf. Table 2).

new relatively weak band at ca. 620 nm, a slight intensity increase at ca. 495 nm, and a more-pronounced shoulder at ca. 560 nm are observed (Figure 5B). These changes are paralleled by an intensity decrease of the 695-nm absorption band indicating the breakage of the Fe−Met-80 bond.

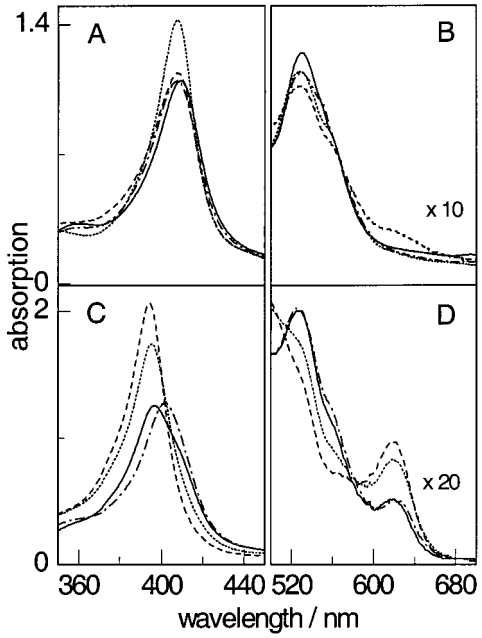

Figure 5. UV−vis absorption spectra of ferric Cyt-*c*. The top panels show Cyt-*c* in aqueous solution at pH 7.0 (—), in 2 mM SDS (···), in DOPG suspensions with a DOPG/Cyt-*c* ratio of 50:1 (− − −), and in aqueous solution at 70 °C and pH 7.0 (− · −). The Soret-band and visible regions are shown in panels A and B, respectively. The bottom panels show Cyt-*c* in aqueous solutions at low ionic strength and pH 2.4 (—), pH 0.8 (···), and pH 1.3 (− − −), and in solution of high ionic strength (2 M NaCl) at pH 1.5 (− · −). The Soret-band and visible regions are displayed in panels C and D, respectively.

Binding to DOPG vesicles causes an upshift of the RR marker band positions and a decrease of the ν_{10} band intensity (Figure 6C) similar to those of the nonnative 6cLS configuration prevailing in 2 mM SDS solutions (Figure 6D). Furthermore, at DOPG/Cyt-*c* ratios ≥50:1, the peaks in the marker band region become increasingly broadened and asymmetric with distinctly higher intensities on the low-frequency sides, which is most clearly seen for the ν_3 and ν_2 peaks. These findings as well as the concomitant increase of a 620-nm absorption band at high DOPG/Cyt-*c* ratios point to the formation of HS species as found for Cyt-*c* in SDS solutions above the cmc. To check this conclusion, we have subtracted the RR spectrum of Cyt-*c* measured in the presence of 2 mM SDS from those obtained at high DOPG/Cyt-*c* ratios. In fact, the resultant difference spectra

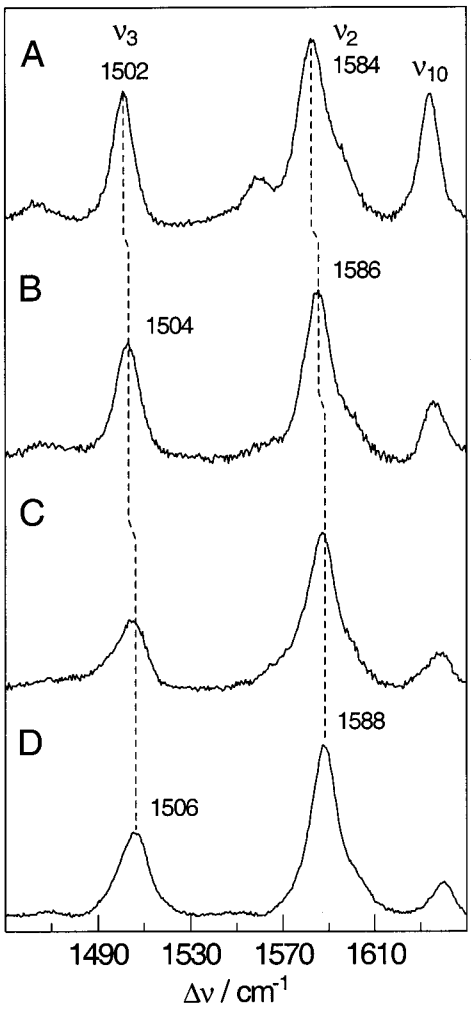

Figure 6. RR spectra of ferric Cyt-*c* in the marker band region between 1450 and 1650 cm^{-1} obtained from (A) aqueous solution (pH 7.0) at 22 °C and (B) at 70 °C and (C) from DOPG suspensions with a DOPG/Cyt-*c* ratio of 50:1 and (D) in 2 mM SDS solution at pH 7.0. The spectra were obtained with 413-nm excitation.

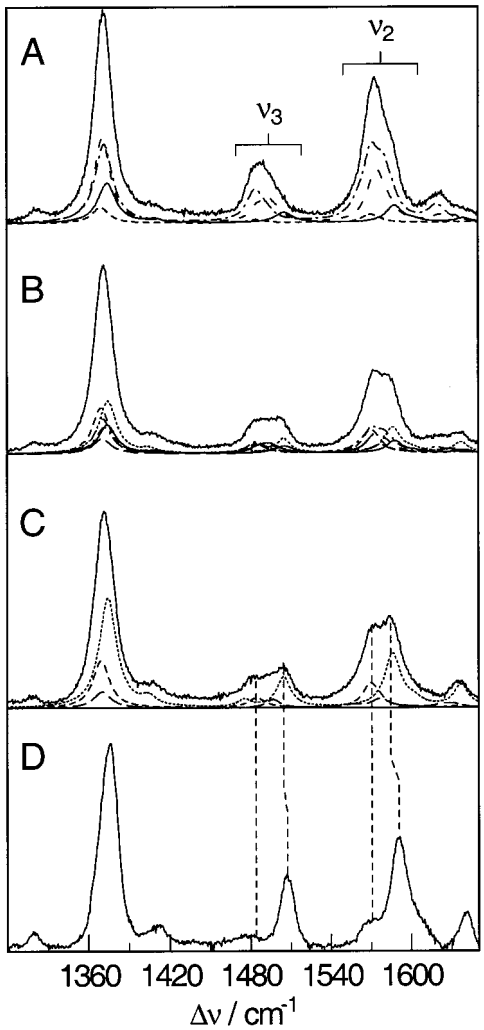

Figure 7. RR spectra of ferric Cyt-*c* in the marker band region between 1300 and 1650 cm^{-1}, obtained from acid solutions at low ionic strength (A) at pH 1.3 and (B) at pH 0.8 and (C, D) at high ionic strength (2 M NaCl) at pH 1. Spectrum C was recorded at room temperature, while spectrum D was obtained at −140 °C. All spectra were obtained with 413-nm excitation. The component spectra of the various heme configurations are indicated by different line types: (—) B2[6cLS]; (···) A[6cLS]; (– – –) B2[6cHS(1)]; (– · –) U[6cHS(2)]; (– ···) U[5cHS]; (— — —) B2[5cHS]. Further details are given in the text (cf. Table 2).

display the marker bands that are characteristic of a 5cHS and 6cHS species. Thus, both the RR and UV−vis absorption spectral changes of Cyt-*c* bound to DOPG vesicles are closely related to those of Cyt-*c* induced by SDS, pointing to the formation of similar heme configurations.

Hence, the set of component spectra that were refined in the previous global analyses were then applied to analyze the RR spectra of Cyt-*c* bound to DOPG liposomes. For this system, all measured spectra could be simulated by the component spectra of two 6cLS forms, B1[6cLS] and B2[6cLS], as well as those of B2[5cHS] and U[6cHS(1)] used for the fits to the RR spectra of Cyt-*c* in SDS solutions. No refinement of these component spectra was required to obtain a good global fit to the experimental spectra obtained at different Cyt-*c*/lipid ratios indicating that for the lipid-bound B2 state the RR spectrum of the 6cHS configuration, B2[6cHS], is identical to that of U[6cHS(1)]. Because of the overall low intensity of the 6cHS marker bands, minor contributions from an U[6cHS(2)]-like species cannot be absolutely ruled out, whereas the involvement of the U[5cHS] species can safely be excluded (Table 1). These findings imply that Cyt-*c* binding to DOPG liposomes leads to those heme configurations that were also found in the Cyt-*c*/SDS system.

Spectral Changes of Ferric Cytochrome *c* Induced at Low pH. Regardless of the ionic strength, the 695-nm absorption band of the native LS form decreases between pH 4.5 and 3, whereas characteristic HS absorption bands such as the 620-nm and the 495-nm band gain intensity (Figure 5D). Unlike in neutral aqueous solution, the ionic strength has a distinct effect on the heme pocket structure in highly acidic solution. The blue shift of the Soret band is less-pronounced at high ionic strength (2 M NaCl) with maxima at 401.5 and 400.5 nm at pH 1.5 and 0.5, respectively, whereas at low ionic strength, the Soret band shifts down to 394 nm at pH 1.3 and then up again to 396.5 at pH 0.8 (Figure 5C). Further ionic-strength-dependent differences are noted in the Q-band region as well for the 620-nm band, which at high ionic strength shifts up to 629 nm at pH 0.5 but remains unchanged at low ionic strength.

RR spectroscopy proves the conversion to nonnative states at pH $\approx$ 3 with the HS species becoming the dominant forms at pH $\leq$ 2.5 (Figure 7). At high ionic strength, the prevailing 6cHS form is closely related to that formed in the presence of GuHCl at pH 4.1. However, in acidic solutions (pH 1.3) of low ionic strength, a 6cHS form dominates that resembles that observed only in GuHCl solutions at pH $<$ 4, as indicated by

the characteristic high intensity of the ν_2 marker band. A second substantial difference refers to a new 6cLS configuration that is formed to a considerable extent in the pH range between 2.5 and 0.5 at high ionic strength but may exist, if at all, only in a very low percentage at low ionic strength (Figure 7). Also for this species, the RR marker bands are shifted to higher frequencies compared to the native 6cLS configuration and, in this respect, display the same tendency as observed for the 6cLS configurations in the U and B2 states. These similarities, however, do not include the relative band intensities. In particular, we note a substantially higher ν_{10} band intensity in the "acid" 6cLS form.

The global fit to the RR spectra of ferric Cyt-*c* in acidic solutions requires the component spectra of all high-spin heme configurations, as well as of U[6cLS]. For those spectra measured at high ionic strength, an additional 6cLS configuration had to be taken into account that exhibits spectral parameters that are clearly different from those of U[6cLS] and also differ from that of B1[6cLS], which, in turn, contributes to the measured spectra only at higher pH. As in acidic solutions of high ionic strength, ferric Cyt-*c* is converted to the so-called A-state, the new 6cLS species is denoted as A[6cLS] (Table 1).

In acidic solutions with high ionic strength, lowering the temperature leads to an increase of the contribution of the A[6cLS] species at the expense of the HS forms until at −60 °C the latter can hardly be detected any more (spectrum not shown). At −140 °C, the RR spectrum displays exclusively the A[6cLS] species (Figure 7D). This HS-to-LS transition is fully reversible.

At low ionic strength and ambient temperature, this species gives only minor contributions to the measured spectra. At pH ≤ 1.3, the RR spectra are exclusively dominated by the component spectra of U[5cHS], U[6cHS(2)], and U[6cHS(1)]. Besides these species, the component spectra of U[6cLS], as well as of the B1[6cLS], for pH ≥ 2.5 are required for a consistent fit to all measured spectra (Table 1). For none of these component spectra was an adjustment of the spectral parameters necessary.

UV−Vis Absorption and Resonance Raman Spectral Changes of Ferric Cytochrome *c* Induced at High Temperature. In contrast to ferrous Cyt-*c*, the ferric heme protein undergoes structural changes in neutral aqueous solution upon raising the temperature up to 70 °C. These changes are reflected by a slight blue shift of the peak maximum (Figure 5A). Furthermore, the 695-nm absorption band disappears, indicating the breakage of the Fe−Met-80 bond.[36] The RR spectrum measured at this high temperature is similar to that of the 6cLS form in acidic solutions at high ionic strength both with respect to the band frequencies and with respect to the intensity pattern (Figure 6B). This 6cLS species appears to be in a two-state equilibrium with the native Cyt-*c* as indicated by subtracting the RR spectrum of the ferric Cyt-*c* at ambient temperature from those measured in the temperature range between 30 and 70 °C. The component spectrum of this 6cLS species, T[6cLS] (Figure 4), derived from these difference spectra, as well as that of B1[6cLS], afforded a good global fit to all RR spectra measured in this temperature range (Figure 4). There is no indication of contributions from any other species.

UV−Vis Absorption and Resonance Raman Spectral Changes of Ferrous Cytochrome *c* Induced by SDS, GuHCl, and Phospholipid Vesicles. In ferrous Cyt-*c*, the Soret-band maximum is red-shifted to 415 nm compared to ferric Cyt-*c* and the Q-band region displays two distinct absorption maxima

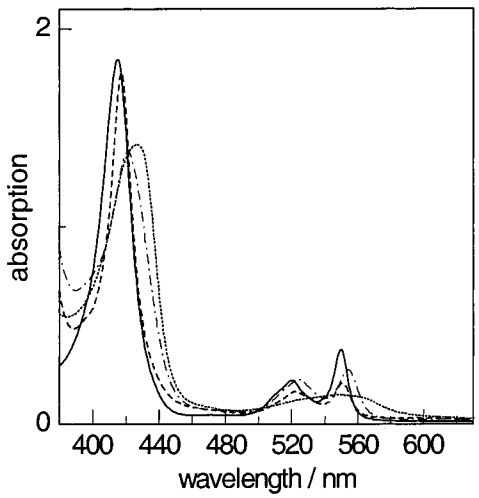

Figure 8. UV−vis absorption spectra of ferrous Cyt-*c* in aqueous solution at pH 7.0 (—), in 250 mM SDS at pH 7.0 (•••), in 10 mM SDS at pH 7.0 including imidazole with an imidazole/Cyt-*c* ratio of 2500:1 (− − −), and in 10 M GuHCl at pH 5.8 (− • −).

at 520 and 550 nm (Figure 8). Upon addition of up to 1.6 mM SDS, only a small upshift of the Soret band by 1 nm is observed accompanied by the appearance of a broad shoulder on the low-frequency side. Increasing the SDS concentration up to 250 mM causes a further broadening and a substantial red shift of the maximum to 428 nm. Furthermore, the characteristic double-banded structure of the Q band is converted to a broad absorption band. The RR spectra indicate that already at SDS concentrations <1.6 mM the native B1[6cLS] species, characterized by the marker bands ν_4, ν_3, ν_2, and ν_{10} at 1361, 1492, 1591, and 1621 cm^{-1}, respectively (Figure 9A), is largely converted to a 5cHS configuration with the corresponding marker bands at 1354, 1470, 1573, and 1606 cm^{-1}, respectively (Figure 9C). This species remains the dominant form also upon further increasing the SDS concentration.

Addition of imidazole to such samples causes a shift of the Soret- and Q-band absorption maxima to 417 and 551 nm, respectively (Figure 8). These changes reflect the formation of a 6cLS configuration as indicated by the characteristic marker bands in the RR spectrum. Because at 10 mM SDS the amount of the formation of this 6cLS species exclusively depends on the imidazole concentration, it is concluded that this substrate serves as an exogenous ligand for the heme iron (Figure 9B).

At pH 5.8, GuHCl induces changes in the UV−vis absorption spectrum of ferrous Cyt-*c* that are similar to those observed in the presence of low SDS concentrations (<1.6 mM) in neutral solution. However, in the case of GuHCl, the RR spectra (spectra not shown) reveal a 6cLS species (U[6cLS]) that is closely related to that of the imidazole complex of ferrous Cyt-*c* (B2[6cLS]) that is formed at high SDS concentrations upon addition of 250 mM imidazole. Compared to the native ferrous 6cLS state, the spectral differences particularly refer to the ν_{11}-mode envelope at ca. 1545 cm^{-1}.

Upon binding to DOPG liposomes at high lipid/protein ratios, distinct changes in the RR spectra are observed. Subtracting the residual 6cLS contributions, a difference spectrum is obtained that displays marker bands at positions characteristic for a 5cHS configuration (Table 2). However, such difference spectra obtained in this way from RR spectra measured at molar DOPG/Cyt-*c* ratios above and below 25:1 are not identical. Specifically, we note a considerable variation of the maximum of the ν_4 band envelope between 1355 and 1358 cm^{-1}, pointing

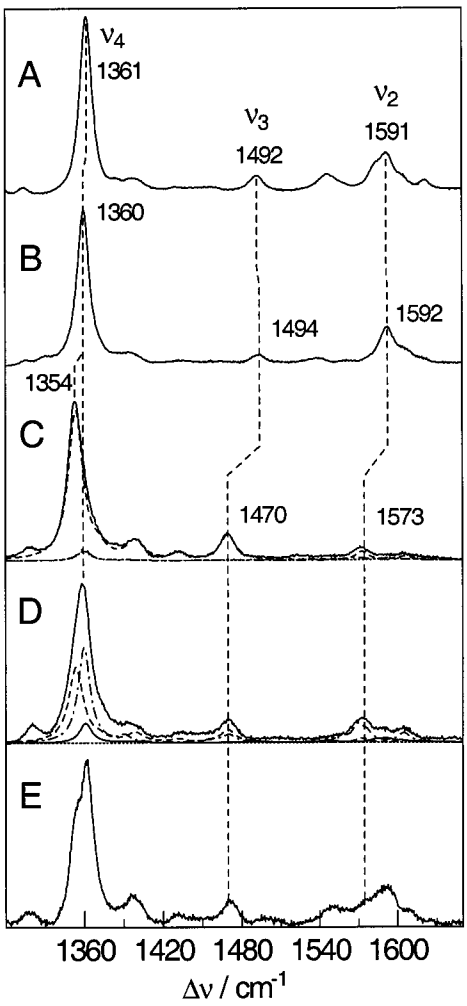

Figure 9. RR spectra of ferrous Cyt-*c* in the marker band region between 1300 and 1650 cm^{-1}: (A) aqueous solution at pH 7.0; (B) solution of 10 mM SDS (pH 7.0) including imidazole with an imidazole/Cyt-*c* ratio of 2500:1; (C) solution of 10 mM SDS (pH 7.0); (D) DOPG suspension with DOPG/Cyt-*c* ratio of 100:1. The component spectra of the various heme configurations in the RR spectra C and D are indicated by different line types: (—) B1[6cLS]; (···) B2[6cLS(1)]; (− − −) B2[5cHS(1)] ; (− · −) B2[5cHS(2)]. Spectrum E is the low temperature ($T = -140$ °C) RR spectrum of slowly frozen ferrous Cyt-*c* (100 μM) in a 100 mM SDS solution. Further details are given in the text (cf. Table 2). All spectra were obtained with 413-nm excitation.

to two different 5cHS species of ferrous Cyt-*c* bound to DOPG.[37]

Subtracting these difference spectra from each other yielded approximate component spectra of the two 5cHS configurations with ν_4 marker band frequencies at ca. 1353 [5cHS(1)] and 1359 cm^{-1} [5cHS(2)]. The B2[5cHS(2)] component spectrum was iteratively refined during the global analysis of the RR spectra of all DOPG/Cyt-*c* complexes. Besides the 5cHS species, B2[5cHS(2)] and B2[5cHS(1)], and the native B1[6cLS] state, this analysis also required an additional 6cLS species, denoted as B2[6cLS], for which the component spectrum was found to be adequately approximated by that of the imidazole complex of ferrous Cyt-*c* in SDS solutions. Note that in imidazole-free solutions of SDS, a nonnative 6cLS species could not be detected for ferrous Cyt-*c* whereas the global analysis indicates the involvement also of the B2[5cHS(2)] species, albeit only to a relatively small extent. The component spectra of all ferrous heme configurations are shown in Figure 10 (Table 2).

Surface-Enhanced Resonance Raman Spectroscopic Changes of Cytochrome *c* Adsorbed on Electrodes. Adsorption of Cyt-*c* in the electrical double layer of a bare Ag electrode causes structural changes in the heme pocket, which are reflected by the SERR spectra. It has already been shown that the underlying conformational transitions are potential-dependent and coupled with electron-transfer reactions between the adsorbed Cyt-*c* and the electrode.[15,18] Adsorption of Cyt-*c* at negative potentials (e.g., −0.4 V) leads to a SERR spectrum that is essentially identical to the RR spectrum of the native ferrous state B1. Upon setting the potential to positive values, >0.0 V, the ferric form of B1 is obtained which, however, is not stable in this potential range but is (partially) converted to nonnative states including a 6cHS, a 5cHS, and a 6cLS configuration. The degree of this conformational conversion increases with increasing potential so that at +0.23 V essentially all of the adsorbed Cyt-*c* exists in the nonnative states. Under these conditions and subsequent lowering of the potential to values less than −0.2 V, back conversion to the native state is slow and occurs within hours.[29] Figure 11B shows a SERR spectrum of such a sample, measured at −0.07 V, in which the nonnative 6cLS species represents the prevailing component as indicated by the prominent marker bands at ca. 1375 (ν_4), 1506 (ν_3), 1588 (ν_2), and 1639 cm^{-1} (ν_{10}). The qualitative inspection of the spectra already reveals the good agreement for the marker band frequencies and intensities of this 6cLS species with the ferric B2[6cLS] state of Cyt-*c* formed in the presence of SDS (Figure 11A). Such similarities also refer to the reduced forms of the nonnative states of the adsorbed Cyt-*c*, a 6cLS and a 5cHS species, which are obtained after setting the potential to values in the range between −0.35 and −0.55 V. However, at such negative potentials, these nonnative states are not stable but are converted back to the reduced 6cLS form of the native B1 state.[29]

The similarities of the conformational changes of the Cyt-*c* induced by adsorption on the electrode and by binding to phospholipid vesicles have been pointed out previously.[11,18] Thus, the B1 and B2 component spectra constitute the starting point for the analysis of the SERR spectra. In the first step of the global analysis, the spectral parameters of those species that could be obtained in a largely pure form were adjusted to account for the specific electric field effects on the vibrational spectra.[18] For the native B1 state, such refinements included only small variations of the relative band intensities and frequency changes of ca. 0.3 cm^{-1}. The simulation of the nonnative ferrous 5cHS and ferric 6cLS components of the SERR spectra was satisfactorily achieved on the basis of the original component spectra of ferrous B2[5cHS(2)] and ferric B2[6cLS] after adopting similarly small adjustments. No additional component spectra of these heme configurations were required for the fit.

On the other hand, the ferric 5cHS and 6cHS, as well as the nonnative ferrous 6cLS, contributions to the SERR spectra could only satisfactorily be reproduced after more pronounced alterations of the original component spectra. Comparable modifications of the spectral parameters were also unavoidable upon including the component spectra of two additional HS states, U[6cHS(2)] and U[5cHS]. Although a good global fit can be achieved solely on the basis of the modified B2[5cHS] and B2[6cHS(1)] component spectra, the involvement of further U-state(-like) HS species cannot be ruled out.

For the nonnative ferrous 6cLS form, the determination of the spectral parameters was associated with a somewhat higher uncertainty because this state only contributes to a relatively small extent to the experimental SERR spectra. The resultant component spectrum of this state is closely related to that of

TABLE 2: RR Spectral Parameters of the Various Nonnative Conformational States of Cyt-*c*[a]

Ferric Heme States

	6cLS				6cHS		5cHS	
mode	B1[6cLS] Met/His	B2[6cLS][b] U[6cLS] His/His	A[6cLS] H_2O/His	T[6cLS] X/His	B2[6cHS] U[6cHS(1)] H_2O/His	U[6cHS(2)] H_2O/H_2O	B2[5cHS] His	U[5cHS] H_2O
ν_4	1372.5 (1.0)	1374.1 (1.0)	1374.5 (1.0)	1375.6 (1.0)	1369.5 (1.0)	1372.0 (1.0)	1370.3 (1.0)	1370.9 (1.0)
ν_3	1501.9 (0.26)	1505.8 (0.25)	1504.7 (0.27)	1504.0 (0.35)	1484.7 (0.20)	1483.9 (0.40)	1496.9 (0.52)	1492.9 (0.24)
ν_2	1583.6 (0.35)	1587.8 (0.50)	1585.9 (0.47)	1585.8 (0.52)	1569.1 (0.44)	1570.3 (0.79)	1576.7 (0.55)	1575.3 (0.45)
ν_{10}	1634.7 (0.25)	1639.6 (0.12)	1637.0 (0.20)	1639.6 (0.12)	nd	1619.4 (0.20)	1622.5 (0.16)	1625.3 (0.05)

Ferrous Heme States

	6cLS			5cHS	
mode	B1[6cLS] Met/His	U2[6cLS] His/His	B2[6cLS][c] His/His	B2[5cHS(1)] $His^{(-)}$	B2[5cHS(2)] His
ν_4	1361.1 (1.0)	1364.8 (1.0)	1360.0 (1.0)	1353.7 (1.0)	1359.9 (1.0)
ν_3	1491.8 (0.10)	1495.6 (0.12)	1494.0 (0.06)	1469.6 (0.17)	1470.6 (0.08)
ν_2	1591.2 (0.19)	1591.0 (0.15)	1592.0 (0.23)	1572.7 (0.06)	1569.6 (0.17)
ν_{10}	1621.0 (0.07)	nd	nd	1606.3 (0.02)	1604.7 (0.10)

[a] Frequencies are given in cm^{-1}; band intensities (in parentheses) refer to the ν_4 mode. [b] The spectral parameters refer to the B2[6cLS]. For U[6cLS], the frequencies (relative intensities) of modes ν_4, ν_3, ν_2, and ν_{10} are 1374.2 (1.0), 1505.4 (0.25), 1587.6 (0.42), and 1639.0 cm^{-1} (0.10), respectively. [c] The spectral parameters are very similar to those determined for the imidazole complex of ferrous Cyt-*c* in SDS solutions.

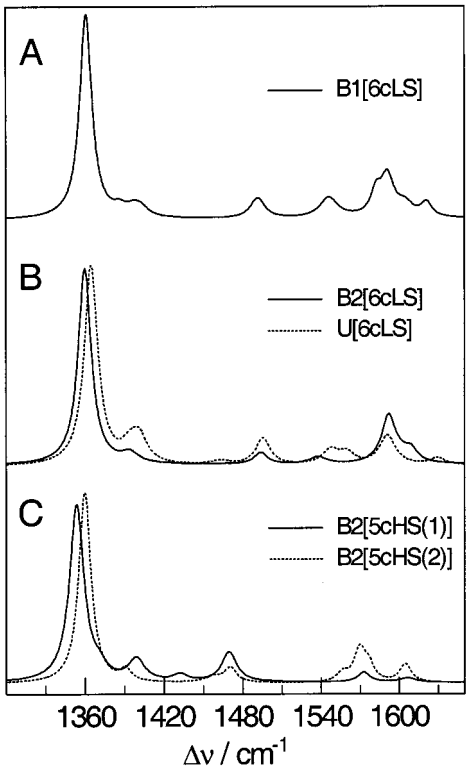

Figure 10. Component RR spectra of the ferrous Cyt-*c* species in the marker band region between 1300 and 1650 cm^{-1}: (A) (—) B1[6cLS]; (B) (—) B2[6cLS] and (···) U[6cLS]; (C) (—) B2[5cHS(1)] and (···) B2[5cHS(2)]. Further details are given in the text (cf. Table 2).

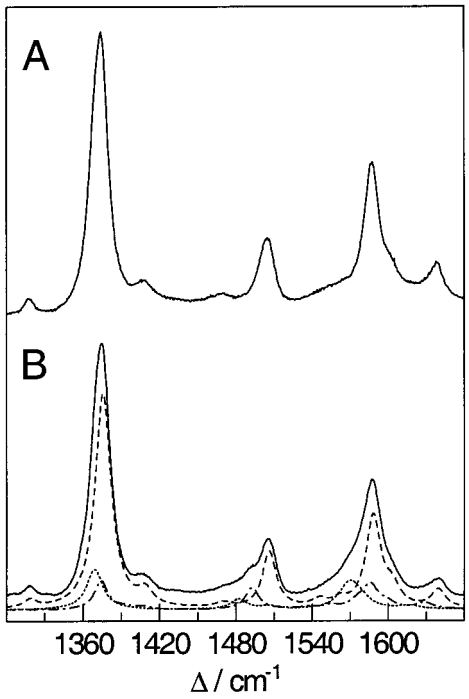

Figure 11. RR spectrum (A) of ferric Cyt-*c* (yeast iso-1) in a 2 mM SDS solution (pH 7.0) and SERR spectrum (B) of Cyt-*c* (yeast iso-1) adsorbed on an Ag electrode at −0.07 V after a residence time of ca. 10 s [29] at + 0.23 V. In spectrum B, the solid, dashed, and dotted lines denote the component spectra of ferric B2[6cLS(1)], B2[6cHS(1)], and B2[5cHS(1)], respectively. The RR and SERR spectra were measured with 413-nm excitation. Further details are given in the text.

the imidazole complex of ferrous Cyt-*c* in SDS solutions (B2[6cLS]). On the basis of these refined component spectra of the B1 and B2 states, a consistent fit to ca. 80 experimental SERR spectra was achieved.

Identification of the Axial Ligands of the Nonnative Heme Configurations. RR and SERR spectra can distinguish those conformational states of Cyt-*c* that differ by their heme structures, that is, the geometry of the porphyrin, the spin and ligation state, and the kind of the axial ligands.[34,38−40] The various heme configurations that have been characterized by RR/SERR spectroscopy exist in quite different systems, implying that the same changes of the heme structure of Cyt-*c* can be induced, for instance, by interactions with GuHCl or SDS or by binding to DOPG liposomes.

Using site-specifically mutated Cyt-*c* variants, Colòn et al. have demonstrated that in neutral GuHCl solution His-33 (or His-26) substitutes for the native Met-80 heme ligand to give a 6cLS configuration.[41] Furthermore, it was shown that upon lowering the pH GuHCl-denatured ferric Cyt-*c* is first converted into a 6cHS form with a pK_a of 5.2, and at an even lower pH (pK_a = 3.8) into a 5cHS species.[4,6,27,42] The 6cHS species was assigned to a His−H_2O configuration with the native His-18

ligand remaining coordinated to the heme, whereas His-33 is replaced by a water molecule. The 5cHS species dominating at low pH was originally assigned to a His-18 ligated form.[42] However, on the basis of the analysis of the protein-folding kinetics[27] and comparative RR spectroscopic studies on microperoxidase[43] and heme model compounds,[44] Rousseau and coworkers provided evidence for a water molecule as the axial ligand. This assignment was specifically supported by the relatively high ν_4/ν_3 intensity ratio (>4), which for His (or imidazole)-coordinated 5cHS species is much lower (<2) upon Soret-band excitation.[44]

On the basis of these results, it is straightforward to assign the axial ligands in the U-state heme configurations U[6cLS] and U[5cHS] characterized in this work to His-33/His-18 and H_2O, respectively. In contrast to previous studies,[6,45] we have detected two 6cHS species. One of them, U[6cHS(1)], prevails in the pH range between 5 and 4 and, hence, is attributed to a H_2O/His-18-ligated heme as suggested by Yeh et al.[6,45] The second 6cHS species, U[6cHS(2)], is found at lower pH and exists in considerable amounts at pH values down to pH 2 and, therefore, is ascribed to a bis-aquo-coordinated heme. These assignments are consistent with the quantitative analysis of the RR spectra measured in GuHCl in the range from pH 7 to pH 0. For the dissociation of the first His (His-33) from the heme iron, corresponding to the transition from U[6cLS] to U[6cHS(1)], a pK_a of 5.3 was determined, which is nearly identical to that found for the protonation of His-33.[6,27] The pK_a for the dissociation of the second His (His-18), which corresponds to the formation of U[6cHS(2)] and U[5cHS], was determined to be 3.4, which also compares very well with the reported value of 3.8.[6,27]

As discussed above, the ferric B2[6cLS] configuration detected in SDS solutions exhibits essentially the same RR and UV−vis absorption spectra as U[6cLS] in GuHCl solutions (Figure 1, Table 2). For instance, the marker band frequencies deviate by less than 0.4 cm^{-1} and the relative band intensities by less ca. 8%. This very good agreement suggests the same axial ligands for B2[6cLS] and U[6cLS]. To check this conclusion, we have employed EPR spectroscopy (Figure 12). The EPR spectrum of the native ferric B1 state exclusively displays the LS signals with g_1, g_2, and g_3 values of 3.03, 2.25, and 1.18, respectively. The EPR spectra of Cyt-*c* in SDS (100 mM; pH 7) and GuHCl solutions (6 M, pH 5) include both LS signals and a strong $g \approx 6$ signal that originates from HS species formed at high SDS concentrations and slightly acidic GuHCl solutions. Compared to native Cyt-*c*, the LS signals of Cyt-*c* in SDS and GuHCl are characterized by a distinctly lower value for g_1 of 2.93 and can be simulated by the same set of *g* values. Note that these *g* values agree very well with those reported for a Cyt-*c*/imidazole complex[46] or bis-His-coordinated microperoxidase,[47] indicating that they are characteristic of such a ligation pattern. Furthermore, also the Soret-CD spectra of B2[6cLS] and U[6cLS] are similar (vide infra). Thus, the excellent agreement of the UV−vis absorption, RR, EPR, and Soret-CD spectra, which constitute a spectral fingerprint of the heme configuration including the kind of the axial ligands, leads to the conclusion that both states possess the same axial ligands, His-33 and His-18. Most likely, this coordination pattern also holds for the ferrous B2[6cLS] configuration in view of the spectral similarities with the imidazole complex of ferrous Cyt-*c* in SDS solutions. This conclusion is also in line with the fact that the ferrous B2[6cLS] state adsorbed on the electrode forms an ideal Nernstian redox couple with the ferric B2[6cLS] species.[18,29]

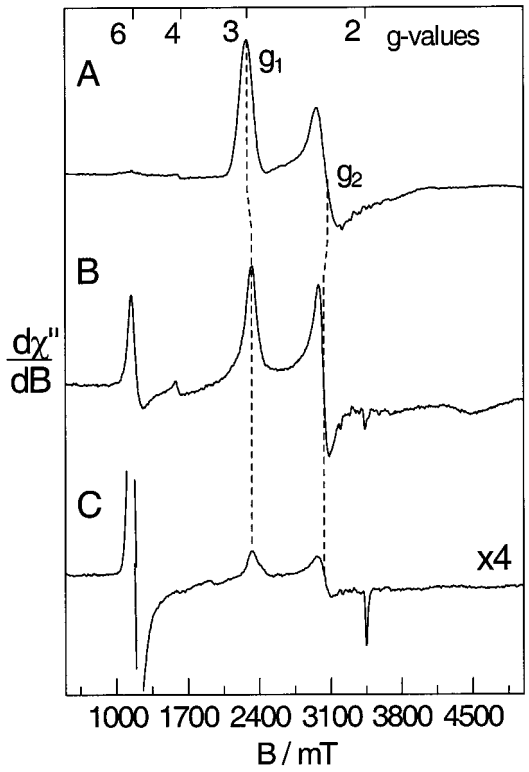

Figure 12. EPR spectra of ferric Cyt-*c* at 10 K: (A) aqueous solution, pH 7.0; (B) 100 mM SDS solution, pH 7; (C) 6 M GuHCl solution at pH 5.

On the basis of the present results, it is necessary to revise our previous assignment for the sixth ligand in the 6cLS form of ferric B2. In earlier studies, this ligand was attributed to a hydroxide in view of the similar, albeit not identical, RR spectrum of the Cyt-*c* state that prevails in highly alkaline solutions (pH > 10).[17] These similarities particularly refer to the frequency upshifts of the marker bands and the substantial intensity decrease of the ν_{10} mode. Taking into account the currently available experimental data, it must be pointed out that these tendencies reflect quite generally the replacement of a weak ligand (Met) by a stronger one, and, hence, per se, are not sufficient for the assignment to a specific ligand.

The H_2O-ligated U[5cHS] state is only formed at very low pH, obviously following the protonation of the native His-18 ligand. In contrast, the B2[5cHS] form exists around pH 7, for example, in the Cyt-*c*/SDS or Cyt-*c*/DOPG systems so that the protonation of His-18 and its subsequent substitution by a H_2O molecule is unlikely. Moreover, the low ν_4/ν_3 intensity ratio of ca. 2 indicates that the heme iron is coordinated by a strong field ligand so that the fifth ligand of B2[5cHS] is ascribed to His-18.[44]

It is very likely that the same ligation pattern holds for the ferrous species because they are formed also under relatively mild conditions, that is, upon binding to DOPG, which does not affect the secondary structure. The main difference between both species refers to the ν_4 mode, which is known to be a sensitive indicator for the electron density in the porphyrin.[40] An increase of electron density, which can be induced by electron-donating axial ligands, is reflected by a frequency downshift of this mode. Therefore, the lowering of the ν_4 frequency by ca. 6 cm^{-1} from B2[5cHS(2)] to B2[5cHS(1)] is likely to reflect an increased electron-donating capability of the axial ligand, which, in turn, may result from stronger hydrogen-bond interactions of the N−H group of the imidazole ring.[48] In the native state of Cyt-*c*, this group forms a hydrogen bond

TABLE 3: Heme Configurations and Protein Structural Changes in the Various States of Cyt-*c*

		protein structure		heme configurations	
state	system	secondary structure	heme pocket structure	ferric	ferrous
B1	neutral solution	native structure preserved	native structure preserved	B1[6cLS], Met-80/His-18	B1[6cLS], Met-80/His-18
B2	electrode (<0.1 V); DOPG; SDS (>cmc)[a]	native structure preserved	main changes in upper part; open structure	B2[5cHS], His-18; B2[5cHS], His-18; B2[6cLS], His-33/His-18	B2[5cHS(1)], His-18$^{(-)}$; B2[5cHS(2)], His-18; B2[6cLS], His-33/His-18[b]
T	neutral solution at $T = 70$ °C	moderate loss of ordered structure	main changes in upper part; open structure	T[6cLS], X/His-18	
A	low pH and high ionic strength	moderate loss of ordered structure	main changes in upper part; open structure	A[6cLS], H_2O/His-18	
U	GuHCl; low pH and low ionic strength	complete loss of ordered structure	complete loss of ordered structure	U[6cLS], His-33/His-18; B2[5cHS], His-18; U[6cHS(1)], H_2O/His-18; [6cHS(2)], H_2O/H_2O; U[5cHS], H_2O	U[6cLS], His-33/His-18[c]

[a] Binding of Cyt-*c* to SDS below the cmc leads to a moderate loss of the secondary structure. [b] Not oberserved in the SDS/Cyt-*c* system. [c] Only observed in the GuHCl/Cyt-*c* system.

with Pro-30.[49] Small structural rearrangements in this part of the heme pocket may affect hydrogen-bonding interactions of His-18 and may eventually lead to an increase of the net negative charge on this ligand. In fact, low-temperature experiments with the SDS/Cyt-*c* system have shown that the reversible transition from ferrous B2[5cHS(1)] only occurs upon slow cooling (Figure 9E) but is hindered upon shock freezing (spectrum not shown), confirming the view that the transition between ferrous B2[5cHS(1)] and B2[5cHS(2)] requires structural alterations in the heme pocket.

Previous studies on the A-state of ferric Cyt-*c* do not provide a consistent picture of the axial ligands in the A[6cLS] configuration. The preservation of the Fe−Met-80 bond, as proposed by Goto et al.[50] and Santucci et al.,[51] is in contradiction to the lack of the 695-nm charge-transfer band (Figure 5D) and other spectroscopic results.[52−54] Alternatively, Jordan et al.[28] and Indiani et al.[55] suggested the replacement of Met-80 by a water ligand corresponding to the same H_2O/His ligation pattern as in the ferric [6cHS(1)] form but adopting a low-spin configuration. This assignment is supported by the present temperature-dependent studies that have demonstrated a temperature-dependent equilibrium between the U[6cHS(1)] and the A[6cLS] species.[56] Evidently, at low temperature, the thermal energy is not sufficient to overcome the energy difference between the t_{2g} and e_g orbitals.

For the T[6cLS] configuration of ferric Cyt-*c*, the identification of the sixth ligand is not unambiguous.[36,57,58] On the basis of NMR signals of the heme methyl substituents similar to those observed for the alkaline state IV of Cyt-*c*, Taler et al.[57] proposed a lysine residue as the sixth ligand. Comparable analogies are not found for the RR spectra when the Lys-73- and Lys-79-ligated alkaline states (IVa, IVb) are compared with T[6cLS] in the high- and low-frequency region.[17,59] Conversely, state T[6cLS] exhibits more similarities with the A[6cLS] state not only in the RR spectra but also in the Soret-CD spectra (vide infra). However, a H_2O/His-ligated 6cLS configuration that is stable at high temperatures would be somewhat surprising because in the A-state such a ligation pattern leads to a 6cHS configuration even at ambient temperature. The axial ligation patterns of all heme configurations are summarized in Figure 13 and Table 3.

Protein and Heme Structural Changes. Although Cyt-*c* adopts the same heme configurations in the various systems, the accompanying structural changes of the protein may differ substantially. These structural changes occur on the secondary and tertiary structure level and can be probed by CD spectroscopy.

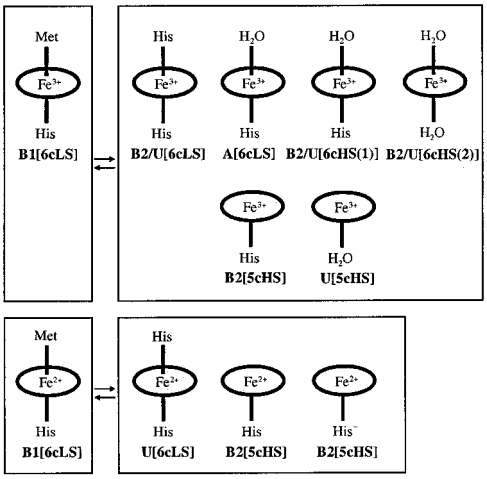

Figure 13. Schematic representation of the various ferric and ferrous heme configurations in the B1, B2, U, and A states as detected in this work.

In the far-UV CD spectrum, native ferric Cyt-*c* exhibits a positive maximum at around 195 nm and two negative maxima at 220 and 209 nm (spectra are not shown). The two minima are typical features for an α-helical structure, which is the dominating secondary structure element of native Cyt-*c* (∼40%). Addition of GuHCl (6 M) causes a complete unfolding of the protein.[50,60] Similar large-scale protein structural changes occur in acid aqueous solutions at low ionic strength.[50,61,62] Conversely, no substantial changes of the secondary structure are induced upon binding to DOPG vesicles as indicated by the largely unchanged ellipticity at 220 nm in the far-UV CD spectra,[37] thereby confirming previous IR spectroscopic studies.[63,64]

Among the various heme configurations detected in this work, some of them are only found under denaturing conditions (GuHCl or low pH) (i.e., the ferric bis-aquo and mono-aquo HS species U[6cHS(2)] and U[5cHS] (Table 1)). These are the only species that lack the native His-18 ligand implying that the underlying structural rearrangements on this side of the heme require a far-reaching degradation of the overall secondary structure. Note that for ferrous Cyt-*c* there is no indication of a replacement of His-18 even in GuHCl (at pH > 3). This may be due to a higher protein stability, which prevents a complete unfolding, or a stronger coordinative Fe−His bond, which persists even in the absence of an appropriate protein fold in the immediate environment. Conversely, upon binding to DOPG liposomes, that is, under nondenaturing conditions, the heme

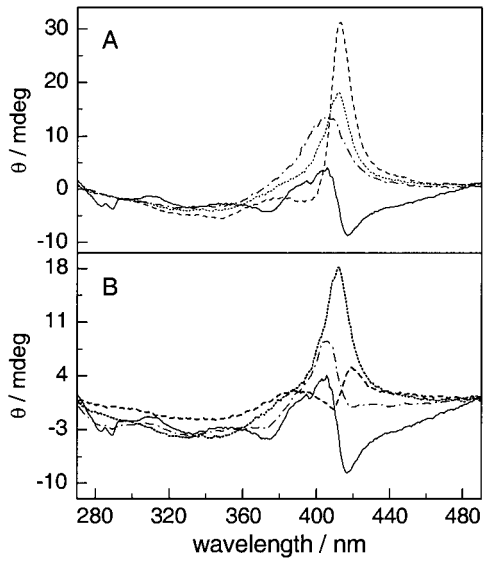

Figure 14. CD spectra of ferric Cyt-*c* between 270 and 500 nm measured at pH 7.0: (A) Cyt-*c* in aqueous solution (—), in 1.2 mM SDS (– – –), in 2 mM SDS (···), and in 10 mM SDS (– · –); (B) Cyt-*c* in aqueous solution (—), in 2 mM SDS (···), and in DOPG suspensions with a DOPG/Cyt-*c* ratio of 50:1 (– – –).

pocket structural changes cause the formation of heme configurations that all possess the His-18 ligand.

For ferric Cyt-*c* in the presence of SDS below the cmc, a loss of secondary structure of about 25% can be observed,[35,37] as indicated by the intensity decrease of the dichroitic band at 220 nm (data not shown), whereas at SDS concentrations above the cmc, a refolding of the protein is noted. Obviously, the secondary structure changes in SDS solutions leave the bottom part of the heme pocket largely intact because only a small contribution the U[6cHS(2)] species that lacks the His-18 ligand could be detected in the RR spectra. We interpret these results in terms of a distribution between a relatively small number of largely unfolded protein molecules, in which the heme is in the U[6cHS(2)] configuration, and a major fraction of Cyt-*c* molecules that suffer only a moderate degradation of the secondary structure without significant perturbation of the bottom side of the heme pocket.

The only heme configurations that are populated to a significant extent under both denaturing and nondenaturing conditions are the ferric and ferrous bis-His-ligated 6cLS species and the ferrous mono-His-ligated 5cHS species. The ferric bis-His-ligated 6cLS configuration can be formed up to 100% in GuHCl solutions at a pH of ca. 7 and even exists in considerable quantities down to pH 4. Thus, it appears to be that the coordination of His-33 leads to an energetically favored species and, moreover, stabilizes the coordinative Fe−His-18 bond. Note that despite the drastic secondary structure changes in GuHCl, the RR spectrum of this species is nearly identical to that measured in SDS solution implying that changes in the protein environment have little affect on the vibrational band pattern in the frequency range between 1300 and 1650 cm^{-1}.

Tertiary-structure changes in the heme pocket are revealed by CD spectroscopy in the regions of the Soret band and between 250 and 300 nm. The latter part of the spectrum probes the molecular environment of the single Trp-59,[65] which is part of the hydrogen-bonded network on the Met-80 side of the heme.[49] The two sharp minima at 282 and 288 nm in the near-UV CD spectrum of native ferric Cyt-*c* (Figure 14) indicate a tight tertiary structural packing in the vicinity of Trp-59. These bands disappear in the presence of GuHCl and SDS concentrations higher than 0.7 mM, respectively. In the Soret-band region, the CD spectrum of native ferric Cyt-*c* in aqueous solution displays an S-shaped feature with a minimum and maximum at ca. 417 and 406 nm (Soret−Cotton effect; Figure 14). These signals are considered to represent a characteristic fingerprint for the integrity of the heme pocket structure because they originate from the coupling of the electronic transition dipole moments of the heme and nearby aromatic amino acids. These amino acids (Trp-59, Tyr-67, Phe-82) are located on the Met-80 side of the heme so that changes in the Soret-CD spectrum should specifically reflect structural perturbations of this part of the heme pocket. Upon addition of SDS, the negative band at ca. 417 nm disappears, and below the cmc, the positive 406-nm band is shifted to ca. 412 nm, accompanied by a strong intensity increase. Raising the SDS concentration above the cmc results in an intensity decrease of the 412-nm band, and the positive band is shifted back to ca. 405 nm. These spectra are closely related to those reported for ferric Cyt-*c* in the presence of GuHCl, which display a single positive and relatively intense band at ca. 408 nm.[66] This agreement in the Soret-CD and near-UV CD spectra indicates that, despite the difference in the overall secondary structure, the conformational changes in the upper part of the heme pocket of ferric Cyt-*c* in GuHCl and SDS solutions are quite similar.

The heme pocket structure changes of Cyt-*c* bound to DOPG are different from those observed for the other systems. The Soret- and near-UV CD spectra of Cyt-*c*/DOPG complexes reveal a different picture inasmuch as the minimum at ca. 417 nm is replaced by two maxima at around 393 and 417 nm (Figure 14). Furthermore, the Trp signals disappear only at DOPG/Cyt-*c* ratios > 17:1, which parallels the formation of the B2[5cHS] species.[37] Thus, the transition to this heme configuration may be associated with an opening of the heme crevice, which in turn lowers the hydrophobicity of the Trp-59 environment.

For Cyt-*c* adsorbed on the Ag electrode, structural changes of the protein cannot directly be probed, because the only applicable spectroscopic method is the SERR technique. The very small differences in the SERR spectra of the native states, as well as of the ferric B2[6cLS] and ferrous B2[5cHS] species, may be either attributed to the electrochemical Stark effect or to subtle electric-field-induced perturbation of the heme pocket.[18] Specific electric-field-induced structural changes may particularly account for the more pronounced spectral deviations of the spectral parameters of the ferric HS species B2[6cHS(1)] and B2[5cHS] from the corresponding counterparts in solution. The ferric HS species of the adsorbed Cyt-*c* may exhibit a higher structural flexibility of the heme pocket because of the lack of one coordinating amino acid and, hence, may respond more sensitively to the strong electric fields in the electrode/electrolyte interface (vide infra).

The SERR spectra do not provide any evidence for an unfolding of the protein, particularly, because those U-state configurations that lack the His-18 ligand are not detectable. Thus, in analogy to Cyt-*c*/DOPG and Cyt-*c*/SDS complexes, the main protein structural changes of Cyt-*c* on the Ag electrode are likely to be confined to the heme pocket, specifically to the Met-80 side of the heme. Only under specific conditions, that is, at potentials greater than +0.2 V, there are indirect indications for more extended protein structural changes. Whereas, in general, the conformational transitions proceed on the millisecond time scale, for a portion of the B2 species formed at such positive potentials, the back conversion to the native state at potentials less than −0.2 V (or even after desorption) occurs,

if at all, with a drastically slower rate.[29] This fraction of the B2 species may have undergone structural changes in the protein, which are presumably remote from the heme pocket because SERR spectra do not indicate any heterogeneity for the B2 heme configurations.

The A-state has already been characterized by a variety of experimental techniques, which all indicate a relatively compact protein structure in which the α-helical content is only reduced to 27−30% compared to the native state.[28,55,67,68] The near-UV CD spectrum displays the characteristic dichroitic peaks of Trp-59, although the ellipticity is reduced compared to the native state.[69] These findings, as well as fluorescence experiments, indicate that Trp-59 remains in vicinity to the heme and the heme pocket adopts a closed structure.

For ferric Cyt-*c* at elevated temperatures, there are striking similarities with the A-state, which not only include the moderate decrease of ordered secondary structure but also refer to the heme pocket. The Soret-CD spectrum of ferric Cyt-*c* at 70 °C, which displays a decrease of the 417-nm minimum and a single positive peak at ca. 406 nm (Figure 14), is reminiscent of that reported for Cyt-*c* in acidic solution at high ionic strength,[54,69] corroborating the RR spectroscopic similarities discussed above. These findings point to similar heme pocket structures (vide supra) in the T[6cLS] and A[6cLS] states, which however is in contrast to conclusions derived from previous investigations on the temperature-dependent conformational changes of ferric Cyt-*c*.[58,70] Clearly, further studies are required to reconcile the various experimental data.

Structural Changes Induced by Electrostatic and Hydrophobic Interactions. In previous studies, it was shown that on electrodes the formation of the conformational state B2 of the adsorbed Cyt-*c* is induced by electrostatic interactions that obviously include two contributions.[71] A locally confined contribution results from Coulombic interactions between the cationic lysine-rich binding domain around the exposed heme edge and the negative charges on the metal surface that could either be specifically adsorbed anions or the headgroups of self-assembled monolayers (SAM) of carboxylate-terminated thiols. Furthermore, the potential drop across the electrode/electrolyte interface corresponds to an electric field, the strength of which depends on the electrode potential and the distance from the electrode. In fact, the portion of B2 formed upon binding of Cyt-*c* to SAMs has been shown to increase with decreasing chain length of the thiols, that is, with increasing electric field strength.[71] Correspondingly, the upshift of the electrode potential, which causes an increase of the electric field strength by enlarging the difference to the potential of zero charge [ca. −0.97 V],[72,73] is accompanied by a shift of the conformational equilibrium toward the B2 state. Also, the distribution among the various B2 species is electric-field dependent inasmuch as the B2 high-spin species, B2[5cHS] and B2[6cHS(1)], are the preferred ferric heme configurations at high electric field strengths.

This interpretation is consistent with the results obtained for Cyt-*c* complexes with DOPG liposomes and SDS micelles at high DOPG/Cyt-*c* ratios and SDS concentrations above the cmc, respectively. Under these conditions, interactions are electrostatic in nature, and we note a substantial population of the ferric B2[5cHS] and B2[6cHS(1)], as well as of the ferrous B2[5cHS(2)], forms. The contributions of these species decrease when, upon lowering the DOPG/Cyt-*c* ratio, protein binding also occurs via hydrophobic interactions.[37] This effect is even more pronounced in the Cyt-*c*/SDS system below the cmc in which hydrophobic interactions prevail. Under these conditions, no B2 high-spin species are observed for ferric Cyt-*c*, which is exclusively converted to the bis-His-coordinated B2[6cLS] configuration. Because the substitution of Met-80 by His-33 requires, at first, the opening of the heme pocket to allow His-33 to approach the heme iron, a plausible site for the hydrophobic attack is the small nonpolar patch on the front surface of Cyt-*c*, which is located just in the center of the pericycle formed by the lysine residues involved in electrostatic binding. This peptide segment includes the (partially) exposed amino acids Ile-81, Phe-82, Ala-83, Gly-84, and Ile-85, and hence, it is directly linked to the Met-80 ligand. Thus, it is conceivable that a subtle movement of this segment, brought about by the hydrophobic interactions, may facilitate the dissociation of the Fe−Met-80 bond (in ferric and ferrous Cyt-*c*) and the subsequent coordination of His-33 in ferric Cyt-*c*.

The present results have shown that electrostatic and hydrophobic interactions with the front surface of Cyt-*c* can cause very similar changes in the heme pocket, that is, the ferric B2[6cLS] species, without any major alterations of the protein structure. Conversely, electrostatic interactions are required to stabilize the ferric B2 HS species, as well as the dissociation of the Met-80 ligand in ferrous Cyt-*c*. The differences between these modes of interactions also suggest that the bis-His-coordinated B2[6cLS] represents an energetically favored species. The preferred formation of this species may partially be due to a high intrinsic stability of a bis-His-coordinated ferric heme complex, which is also reflected by the fact that this heme configuration, U[6cLS], also exists in the fully denatured protein in which it is considered to be a kinetic trap of the refolding process.[3−5]

Nonnative States and Biological Processes of Cytochrome *c*. Biological membranes or binding domains of proteins are capable of exerting electrostatic and hydrophobic interactions so that the B2 species may be formed under physiological conditions. In fact, in the nonreactive fully oxidized complex of Cyt-*c* and its natural partner protein CcO, the ferric bis-His-ligated B2[6cLS] species has been detected,[10,11] implying that the predominantly electrostatic interactions between these proteins are principally sufficient to induce the formation of B2 species. Moreover, the portion of B2 formed in the complex with CcO under equilibrium conditions correlates with the maximum rate constant for the reduction of CcO as determined by steady-state kinetics.[10,11] For the reactive ferrous Cyt-*c*, analogous conformational changes have not yet been detected so that it remains to be checked whether the interprotein electron transfer is gated by the intermediate formation of the ferrous B2 species.[11] On the other hand, it is possible that the transition to a ferric B2 species after the interprotein electron transfer prevents the back reaction due to the drastically lowered redox potential.[74] At least, for the ferric state, the conformational transition between the (native) B1 and the B2 state may in fact occur within a few milliseconds or shorter, which is within the lifetime of the Cyt-*c*/CcO complex at physiological ionic strength.[8]

Furthermore, the conformational states of Cyt-*c* studied in this work may also be related to its role in apoptosis when the heme protein is transferred from the intermembrane space to the cytosol where it contributes to the activation of caspase-9.[19−21] Through the use of monoclonal antibodies, it has been shown that these processes are associated with structural changes of Cyt-*c* similar to those that occur upon binding to phospholipid vesicles.[22] Specifically, these experiments point to structural changes in the vicinity of Pro-44. In fact, this part of the protein surface also includes His-33 (and His-26) so that this region

must be structurally altered when His-33 substitutes for the Met-80 ligand upon binding to liposomes. It is, therefore, suggested that the formation of the bis-His-ligated B2[6cLS] species, possibly induced during the transmembrane transport into the cytosol, represents the active form of Cyt-*c* in the apoptic processes.

IV. Conclusions

The bis-His-ligated ferric LS heme configuration of Cyt-*c* (B2/U[6cLS]) represents the most stable nonnative configuration that exists within a variety of protein structures. In ferrous Cyt-*c*, formation of this configuration requires major alteration of the secondary structure, whereas otherwise the mono-His-ligated HS configuration (B2[5cHS]) is preferred.

Localized structural changes in the heme pocket are induced by hydrophobic and electrostatic interactions with the peptide segment 81−85 and the lysine residues around the exposed heme edge, respectively. Both modes of interactions induce the ferric bis-His-coordinated LS (B2/U[6cLS]) and ferrous mono-His-coordinated HS species (B2[5cHS(1)], B2[5cHS(2)]), among which the ferric His-coordinated 5cHS (B2[5cHS]) and 6cHS forms (B2[6cHS(1)]) are specifically populated at strong electrostatic fields.

Upon increasing loss of secondary structure, the Fe−His-18 bond of ferric Cyt-*c* is destabilized so that eventually the bis-aquo 6cHS (U[6cHS(2)]) and mono-aquo 5cHS (U[5cHS]) configurations are formed. In acid GuHCl solutions, His-18 dissociation from the heme iron occurs with a pK_A of 3.4. The dissociation of the Fe−His-33 bond of the bis-His-ligated heme is observed with a pK_A of 5.3.

The partial reorganization of the protein structure of ferric Cyt-*c* at low pH and high ionic strength is not associated with reformation of the Fe−Met-80 bond. In the A-state, a water molecule has replaced the Met-80 ligand leading to a 6cHS/6cLS spin equilibrium with the 6cLS species prevailing a low temperature. This A[6cLS] species exhibits far-reaching spectral similarities with the conformational state that is formed in neutral aqueous solution at high temperature. For this state, the sixth ligand replacing Met-80 could not be identified.

Acknowledgment. The authors thank Dr. E. Bill for kind support in EPR experiments. The work was supported by the Volkswagen-Stiftung (I 72826) and the Deutsche Forschungsgemeinschaft (Hi 464/4-2). Yeast iso-1 cytochrome *c* was generously provided by Professor A. G. Mauk, Vancouver.

References and Notes

(1) Lanyi, J. K. *J. Biol. Chem.* **1997**, *272*, 31209.
(2) Fink, A. L. *Annu. Rev. Biophys. Biomol. Struct.* **1995**, *24*, 495.
(3) Elöve, G. A.; Bhuyan, A. K.; Roder, H. *Biochemistry* **1994**, *33*, 6925.
(4) Yeh, S. R.; Takahashi, S.; Fan, B. C.; Rousseau, D. L. *Nat. Struct. Biol.* **1997**, *4*, 51.
(5) Englander, S. W.; Sosnick, T. R.; Mayne, L. C.; Shtilerman, M.; Qi, P. X.; Bai, Y. W. *Acc. Chem. Res.* **1998**, *31*, 737.
(6) Yeh, S. R.; Han, S. W.; Rousseau, D. L. *Acc. Chem. Res.* **1998**, *31*, 727.
(7) Pettigrew, G. W.; Moore, G. R. *Cytochromes c − biological aspects*; Springer-Verlag: Berlin, Heidelberg, 1987.
(8) Scott, R. A.; Mauk, A. G. *Cytochrome c* − A multidisciplinary approach, University Science Books: Sausalito, CA, 1996.
(9) Hildebrandt, P.; Vanhecke, F.; Buse, G.; Soulimane, T.; Mauk, A. G. *Biochemistry* **1993**, *32*, 10912.
(10) Hildebrandt, P.; Heimburg, T.; Marsh, D.; Powell, G. L. *Biochemistry* **1990**, *29*, 1661.
(11) Döpner, S.; Hildebrandt, P.; Rosell, F. I.; Mauk, A. G.; von Walter, M.; Buse, G.; Soulimane, T. *Eur. J. Biochem.* **1999**, *261*, 379.
(12) Weber, C.; Michel, B.; Bosshard, H. R. *Proc. Natl. Acad. Sci. U.S.A.* **1987**, *84*, 6687.
(13) Hildebrandt, P.; Stockburger, M. *Biochemistry* **1989**, *28*, 6722.
(14) Heimburg, T.; Hildebrandt, P.; Marsh, D. *Biochemistry* **1991**, *30*, 9084.
(15) Wackerbarth, H.; Klar, U.; Gunther, W.; Hildebrandt, P. *Appl. Spectrosc.* **1999**, *53*, 283.
(16) Hildebrandt, P. *Biochim. Biophys. Acta* **1990**, *1040*, 175.
(17) Döpner, S.; Hildebrandt, P.; Rosell, F. I.; Mauk, A. G. *J. Am. Chem. Soc.* **1998**, *120*, 11246.
(18) Hildebrandt, P.; Stockburger, M. *Biochemistry* **1989**, *28*, 6710.
(19) Cai, J. Y.; Yang, J.; Jones, D. P. *Biochim. Biophys. Acta* **1998**, *1366*, 139.
(20) Green, D. R. *Cell* **1998**, *94*, 695.
(21) Hengartner, M. O. *Nature* **2000**, *407*, 770.
(22) Jemmerson, R.; Liu, J.; Hausauer, D.; Lam, K. P.; Mondino, A.; Nelson, R. D. *Biochemistry* **1999**, *38*, 3599.
(23) Tanford, C. *The hydrophobic effect: Formation of micelles and biological membranes*; John Wiley & Sons: New York, 1980.
(24) Vincent, J. S.; Levin, I. W. *Biochemistry* **1988**, *27*, 3438.
(25) Rytömaa, M.; Kinnunen, P. K. J. *J. Biol. Chem.* **1995**, *270*, 3197.
(26) Salamon, Z.; Tollin, G. *Biophys. J.* **1996**, *71*, 848.
(27) Yeh, S. R.; Rousseau, D. L. *Nat. Struct. Biol.* **1998**, *5*, 222.
(28) Jordan, T.; Eads, J. C.; Spiro, T. G. *Protein Sci.* **1995**, *4*, 716.
(29) Wackerbarth, H. Ph.D. Thesis, MPI f. Strahlenchemie Mülheim/University of Essen, Germany, 2000.
(30) Döpner, S.; Hildebrandt, P.; Mauk, A. G.; Lenk, H.; Stempfle, W. *Spectrochim. Acta* **1996**, *A52*, 573.
(31) Makinen, M. W.; Churg, A. K. In *Iron Porphyrins*; Lever, A. B. P., Gray, H. B., Eds.; Physical Bioinorganic Chemistry Series, 1, 2, 4; Addison-Wesley Publishing Company: Reading, MA, 1983; Chapter 3, p 141.
(32) Yoshimura, T. *Arch. Biochem. Biophys.* **1988**, *264*, 450.
(33) Myer, Y. P.; Saturno, A. F.; Verma, B. C.; Pande, A. *J. Biol. Chem.* **1979**, *254*, 11202.
(34) Parthasarathi, N.; Hansen, C.; Yamaguchi, S.; Spiro, T. G. *J. Am. Chem. Soc.* **1987**, *109*, 3865.
(35) Das, T. K.; Mazumdar, S.; Mitra, S. *Eur. J. Biochem.* **1998**, *254*, 662.
(36) Ångström, J.; Moore, G. R.; Williams, R. J. P. *Biochim. Biophys. Acta* **1982**, *703*, 87.
(37) Oellerich, S. Ph.D. Thesis, MPI f. Strahlenchemie Mülheim/University of Essen, Germany, 2001.
(38) Alden, R. G.; Crawford, B. A.; Doolen, R.; Ondrias, M. R.; Shelnutt, J. A. *J. Am. Chem. Soc.* **1989**, *111*, 2070.
(39) Smith, W. E. *Methods Enzymol.* **1993**, 482.
(40) Kitagawa, T.; Ozaki, Y. *Struct. Bonding* **1987**, *64*, 73.
(41) Colòn, W.; Wakem, L. P.; Sherman, F.; Roder, H. *Biochemistry* **1997**, *36*, 12535.
(42) Takahashi, S.; Yeh, S. R.; Das, T. K.; Chan, C. K.; Gottfried, D. S.; Rousseau, D. L. *Nat. Struct. Biol.* **1997**, *4*, 44.
(43) Wang, J.-S.; Van Wart, H. E. *J. Phys. Chem.* **1989**, *93*, 7925.
(44) Boffi, A.; Das, T. K.; Della Longa, S.; Spagnuolo, C.; Rousseau, D. L. *Biophys. J.* **1999**, *77*, 1143.
(45) Yeh, S. R.; Rousseau, D. L. *J. Biol. Chem.* **1999**, *274*, 17853.
(46) Gadsby, P. M. A.; Thomson, A. J. *J. Am. Chem. Soc.* **1990**, *112*, 5003.
(47) Santucci, R.; Fiorucci, L.; Sinibaldi, F.; Polizio, F.; Desideri, A.; Ascoli, F. *Arch. Biochem. Biophys.* **2000**, *379*, 331.
(48) Smulevich, G.; Neri, F.; Marzocchi, M. P.; Welinder, K. G. *Biochemistry* **1996**, *35*, 10576.
(49) Bushnell, G. W.; Louie, G. V.; Brayer, G. D. *J. Mol. Biol.* **1990**, *214*, 585.
(50) Goto, Y.; Calciano, L. J.; Fink, A. L. *Proc. Natl. Acad. Sci. U.S.A.* **1990**, *87*, 573.
(51) Santucci, R.; Bongiovanni, C.; Mei, G.; Ferri, T.; Polizio, F.; Desideri, A. *Biochemistry* **2000**, *39*, 12632.
(52) Jeng, M. F.; Englander, S. W.; Elöve, G. A.; Wand, A. J.; Roder, H. *Biochemistry* **1990**, *29*, 10433.
(53) Dyson, H. J.; Beattie, J. K. *J. Biol. Chem.* **1982**, *257*, 2267.
(54) Myer, Y. P.; Saturno, A. F. *J. Prot. Chem.* **1991**, *10*, 481.
(55) Indiani, C.; de Sanctis, G.; Neri, F.; Santos, H.; Smulevich, G.; Coletta, M. *Biochemistry* **2000**, *39*, 8234.
(56) Most likely, the transition from U[6cHS(1)] to A[6cLS] is linked with temperature-dependent structural changes of the protein environment and does not represent a pure spin transition.
(57) Taler, G.; Schejter, A.; Navon, G.; Vig, I.; Margoliash, E. *Biochemistry* **1995**, *34*, 14209.
(58) Filosa, A.; English, A. M. *J. Biol. Inorg. Chem.* **2000**, *5*, 448.
(59) Hildebrandt, P.; Pielak, G. J.; Williams, R. J. P. *Eur. J. Biochem.* **1991**, *201*, 211.
(60) Thomas, Y. G.; Goldbeck, R. A.; Kliger, D. S. *Biopolymers* **2000**, *57*, 29.
(61) Myer, Y. P. *Biochemistry* **1968**, *7*, 765.

(62) Fink, A. L.; Calciano, L. J.; Goto, Y.; Palleros, D. R. *Curr. Res. Protein Chem.* **1990**, 417.
(63) Muga, A.; Mantsch, H. H.; Surewicz, W. K. *Biochemistry* **1991**, *30*, 7219.
(64) Heimburg, T.; Marsh, D. *Biophys. J.* **1993**, *65*, 2408.
(65) Davies, A. M.; Guillemette, J. G.; Smith, M.; Greenwood, C.; Thurgood, A. G. P.; Mauk, A. G.; Moore, G. R. *Biochemistry* **1993**, *32*, 5431.
(66) Pinheiro, T. J. T.; Elöve, G. A.; Watts, A.; Roder, H. *Biochemistry* **1997**, *36*, 13122.
(67) Goto, Y.; Takahashi, N.; Fink, A. L. *Biochemistry* **1990**, *29*, 3480.
(68) Hamada, D.; Kuroda, Y.; Kataoka, M.; Aimoto, S.; Yoshimura, T.; Goto, Y. *J. Mol. Biol.* **1996**, *256*, 172.
(69) Marmorino, J. L.; Pielak, G. J. *Biochemistry* **1995**, *34*, 3140.
(70) Yuan, X. L.; Hawkridge, F. M.; Chlebowski, J. F. *J. Electroanal. Chem.* **1993**, *350*, 29.
(71) Murgida, D. H.; Hildebrandt, P. *J. Phys. Chem. B* **2001**, *105*, 1578.
(72) Valette, G.; Hamelin, A. *J. Electroanal. Chem.* **1973**, *45*, 301.
(73) Shlepakov, A. V.; Sevastyanov, E. S. *Sov. Electrochem.* **1978**, *14*, 243.
(74) Wackerbarth, H.; Murgida, D. H.; Oellerich, S.; Döpner, S.; Rivas, L.; Hildebrandt, P. *J. Mol. Struct.* **2001**, *563*, 51.